ELSEVIER

Journal of Molecular Structure (Theochem) 461–462 (1999) 203–222

THEO CHEM

Theoretical study of electronic and geometric structures of a series of lanthanide trihalides LnX_3 (Ln = La–Lu; X = Cl, F) ☆

Takashi Tsuchiya, Tetsuya Taketsugu*, Haruyuki Nakano, Kimihiko Hirao

Department of Applied Chemistry, Graduate School of Engineering, The University of Tokyo, Bunkyo-ku, Tokyo 113, Japan

Received 20 May 1998; accepted 2 July 1998

Abstract

Ab initio molecular orbital calculations are performed for a series of lanthanide trihalides LnX_3 (Ln = La to Lu; X = Cl, F), with the relativistic effective core potentials of Cundari and Stevens, to characterize the tendency in their electronic and geometric structures. In all the complexes (LnX_3), the planar structure (D_{3h} symmetry) is calculated to be stable through normal mode analyses at the complete active space self-consistent field (CASSCF) levels. In the LnX_3, the number of 4f-electrons increases with increasing the atomic number, and 1.2–1.6 (2.1–2.2) electrons are transferred from Ln to Cl (F); the Ln–X bonds are dominated by charge-transfer but have a significant amount of covalent character that involves the 5d-orbital on Ln. It is also found that, along the lanthanide trihalide series, the first seven f-electrons occupy 4f-orbitals one by one from the lowest one up, while the second seven occupy 4f-orbitals from the highest one down, at the Hartree–Fock level. This occupation mechanism is explained in terms of the self-repulsion interactions between two electrons occupying the same spatial 4f-orbital. The Ln–X bond lengths, net charges, and vibrational frequencies show monotonic variation along the lanthanide series, which corresponds to the *lanthanide contraction*. State-averaged CASSCF calculations are also carried out for $LnCl_3$, in a combination with spin-orbit calculations using the atomic spin-orbit coupling constant for the f-electrons, to investigate the energy splitting of the nearly-degenerate low-lying states in the scheme of L–S coupling.

Keywords: Lanthanide trihalide; Relativistic effective core potential; Spin-orbit coupling; Lanthanide contraction; 4f orbital

☆ Dedicated to Professor Keiji Morokuma in celebration of his 65th birthday.

* Corresponding author. Tel./fax: +81 3 58023757; e-mail: take@qcl.t.u-tokyo.ac.jp

0166-1280/99/$ - see front matter
PII: S0166-1280(98)00461-8

1. Introduction

Through the recent development in theoretical chemistry, the applicability of the state-of-the-art ab initio theory has been extended to lanthanide chemistry. The characteristic of electronic structures in lanthanide atoms is the occupation of 4f-orbitals: the outer-shell 5s, 5p and 6s orbitals are occupied completely in the closed-shell, while the inner-shell seven 4f orbitals are occupied incompletely (0–14) in the open-shell. The difficulty in solving the electronic Schrödinger equation for lanthanide complexes is due to the large number of electrons included, the relativicity, and the near-degeneracy of electronic states caused by different 4f-electron configurations. The effective core potential (ECP) method has opened a new possibility for such many-electron systems, in which the inner-shell electrons are replaced with effective potentials acting on the valence-electrons. This scheme can reduce the number of electrons in the system extensively. In addition, effective potentials can be derived with the inclusion of the relativistic effects. Stoll et al. [1] have proposed a quasi-relativistic pseudopotential for the lanthanides, in which 4f-electrons are replaced with the potential while 5s- and 5p-electrons are explicitly treated, while Ross et al. [2] have reported an Ln ECP scheme in which 54 electrons (a [Xe] core) are replaced by the core potential while 4f-electrons are treated explicitly. Cundari and Stevens [3] have developed relativistic ECP (RECP) for the lanthanide atoms with a 46-electron ([Kr]$4d^{10}$) core, in which 4f-, 5s-, and 5p-electrons are explicitly treated.

The energy level of the ground states of lanthanide atoms with the degeneracy related to several different 4f-electron configurations should split out due to the spin-orbit coupling. The resultant spin-orbit coupled states can be classified by two different schemes, i.e. L–S coupling (Russell–Saunders coupling) or j–j coupling [4], where L and S denote quantum numbers of the total-orbital-angular-momentum and total-spin-angular-momentum, respectively, and j denotes a quantum number of a total angular momentum for each electron. If the spin-orbit interaction is small, the scheme of L–S coupling is valid. Through the L–S coupling, the (L, S) state with $(2L+1)(2S+1)$-fold degeneracy should split into $(2S+1)$ levels (when $L \geq S$); each of them is composed of states with the same value of J $(=L-S,\ldots,\ L+S)$ and is $(2J+1)$-fold degenerate, corresponding to the possible values of M_J $(=-J,\ldots,\ J)$, where J and M_J denote quantum numbers of the total electronic angular momentum and its z-component, respectively. As the atomic number increases, relativistic effects such as the spin-orbit interaction become large, then the scheme of j–j coupling becomes valid. For lanthanide atoms (and complexes), the situation may be intermediate between L–S and j–j coupling. Very recently, Yabushita et al. [5–7] carried out spin-orbit CI calculations on multiplet terms of trivalent lanthanide cations, and obtained fairly good agreement with experiment for the ground LS multiplet splittings.

The unique chemical and physical properties of lanthanides have attracted considerable experimental attention [8–12]. To derive fundamental insight into the electronic structure, chemical bonding, and geometric structures of the lanthanide complexes, we focus here on the relatively simple molecules, LnX_3 (Ln = La to Lu; X = Cl, F). The lanthanide trihalides have been studied both experimentally [13–17] and theoretically [18–24], but there still remain discrepancies in the molecular structures, i.e. a pyramidal C_{3v} or a planar D_{3h} geometry. Cundari et al. [22] performed the unrestricted Hartree–Fock (UHF) and complete active space self-consistent field (CASSCF) calculations, with their RECP [3], for the 56 lanthanide trihalides, LnX_3 (Ln = Ce to Lu; X = F, Cl, Br, I), and located their equilibrium geometry. At the CASSCF level, the planar structure was calculated to be most stable in all the complexes under a C_{3v} symmetry constraint, while at the HF level, CeF_3, PrF_3, and PmF_3 were calculated to be pyramidal structures. They showed that both UHF and CASSCF methods give excellent agreement with experiment for Ln–X bond length, so that the root-mean-square difference between CASSCF/RECP Ln–X bond lengths and those estimated from gas-phase experiments is only 0.05 Å (~ 2%) [22]. Lanza and Fragalà [23,24] determined molecular geometries

and vibrational frequencies of lanthanide trihalides LnX_3 (Ln = La, Gd, Lu; X = F, Cl) by the HF, CASSCF, the singles and doubles configuration interaction (SDCI), and the second order Møller–Plesset (MP2) methods with the RECP [3,25]. Their results are also in good agreement with the experimental values.

In this study, we apply the UHF and CASSCF methods, with the RECP of Cundari and Stevens, to a series of lanthanide trihalides LnX_3 (Ln = La to Lu; X = Cl, F), and determine their equilibrium structures, vibrational frequencies, and electron configurations with lowest energy. State averaged CASSCF (SA-CASSCF) calculations are also carried out, in a combination with spin-orbit calculations using the atomic spin-orbit coupling constant for the f-electrons, to investigate the energy splitting of the low-lying electronic states in the scheme of L–S coupling.

2. Computational methods

Ab initio molecular orbital calculations were performed for a series of lanthanide trihalides, LnX_3 (Ln = La, Ce, Pr, Nd, Pm, Sm, Eu, Gd, Tb, Dy, Ho, Er, Tm, Yb, Lu; X = Cl, F), by the UHF and CASSCF methods using the HONDO 95.1 program package [26]. The RECPs of Stevens et al. [3,27,28] were employed, such that 46 electrons of Ln (1s, 2s, 2p, 3s, 3p, 3d, 4s, 4p, and 4d), 10 electrons of Cl (1s, 2s, and 2p), and 2 electrons of F (1s) were replaced with effective potentials. These RECPs were derived including the relativistic effects, which are important especially for heavy atoms like lanthanide elements. The basis sets [3,27,28] used with the RECPs are of double-zeta quality, i.e. (6s6p4d7f/4s4p2d2f) for Ln (Ce to Lu), (6s6p4d/4s4p2d) for La, and (4s4p/2s2p) for X. Equilibrium geometries were first determined for several spatial- and spin-symmetry states with D_{3h} symmetry by using analytical gradients, then normal mode analyses were performed to check the geometrical stability and to determine vibrational frequencies by the finite difference method with analytical energy gradients calculated at both positive and negative sides of the respective Cartesian coordinates with a step size of 0.001 bohr, at both the UHF and CASSCF levels. In CASSCF calculations, seven 4f-orbitals and related electrons were included in the active space. To check the basis set effect, UHF calculations were carried out for $CeCl_3$ and $PrCl_3$, with the addition of d-polarization function ($\alpha_{Cl} = 0.75$) [29] on Cl atoms.

To examine energy levels of the nearly-degenerate low-lying states of lanthanide trihalides, we carried out SA-CASSCF calculations for the respective LnX_3 (Ln = Ce, Pr, Nd, Pm, Sm, Eu, Tb, Dy, Ho, Er, Tm, Yb; X = Cl, F), with equal weighting on the states included. The active space includes only 4f-orbitals and electrons, and the number of averaging states for LnX_3 was taken to be $(2L + 1)$ where L is a total-orbital-angular-momentum for the ground states of Ln^{3+}. Of course, the spin-orbit splittings of the lowest states of LnX_3 should be substantial as in the case of Ln^{3+}. In this study, we investigated the spin-orbit splittings for $LnCl_3$: the $(2L + 1)$ states of $LnCl_3$ obtained by the SA-CASSCF method were used to set up spin-orbit calculations using the atomic spin-orbit coupling constant for the f-electrons, then the energies of the spin-orbit coupled states were evaluated for the respective $LnCl_3$ based on an L–S coupling scheme [4].

The CASSCF (and SA-CASSCF) calculations were carried out with C_1 symmetry specification on electronic wavefunctions (in D_{3h} symmetry molecular structures), then D_{3h} symmetry representations were assigned for the respective electronic states.

3. Results and discussion

3.1. Electronic and geometric structures

The ground states of lanthanide atoms are known to have the electron configuration,

$$(1s)^2(2s)^2(2p)^6(3s)^2(3p)^6(3d)^{10}(4s)^2(4p)^6(4d)^{10}(4f)^n(5s)^2(5p)^6(5d)^1(6s)^2, \quad (1)$$

for La, Ce, Gd and Lu and

$$(1s)^2(2s)^2(2p)^6(3s)^2(3p)^6(3d)^{10}(4s)^2(4p)^6(4d)^{10}(4f)^{n+1}(5s)^2(5p)^6(6s)^2, \quad (2)$$

for other atoms. In the complex LnX_3, three electrons are expected to be transferred from Ln to three X atoms, forming ionic bonds between Ln^{3+} and three X^-. The triple-charged cation Ln^{3+} is known to have the electron configuration, $\cdots(4f)^n(5s)^2(5p)^6$ ($n = 0$–14), in the ground states (no electron in 5d and 6s orbitals), indicating that the electron is occupied one by one in 4f-orbitals according to the increase of the atomic number. Since seven 4f-orbitals form a nearly-degenerate orbital set, n electrons should occupy f-orbitals according to the Hund rule in the complex, thus the spin multiplicity of LnX_3 can be specified by the number of f-electrons, n. Through the preliminary calculations, it is verified that the other spin states have a relatively high energy for the respective LnX_3 at the HF level. In the following, our discussions will be focused on the most stable spin states, in which only 4f-orbitals of Ln are open-shell orbitals.

In LnX_3, the originally degenerate seven 4f-orbitals of Ln split into a''_2, e′, e″, a'_2, and a'_1 orbitals in D_{3h} symmetry. The electronic states of LnX_3 depend on the way n electrons occupy these seven 4f-orbitals, namely the 4f-electron configuration. We located equilibrium structures of D_{3h} symmetry at the UHF level of theory for all the possible non-degenerate 4f-electron configurations for the respective $LnCl_3$. Table 1 shows their total energies (in Hartree), Ln–Cl bond lengths (in Å), Mulliken charges on Ln, and the expectation values of the square of the spin operator, $\langle S^2 \rangle$. Note that the doubly-degenerate orbitals, e′ and e″, are occupied by even number electrons (0, 2, or 4) since we consider only non-degenerate states at the HF level. The spin contamination is found to be negligible in all cases (the largest deviation of $\langle S^2 \rangle$ from the theoretical value is ~ 0.03). In the respective $LnCl_3$, the Ln–Cl bond length and Mulliken charge are almost constant among the different electron configurations, suggesting that different 4f-electron configurations do not change the bonding mechanism of Ln–Cl. In all cases, the planar structure (D_{3h} symmetry) is verified to be stable through normal mode analyses. The calculated vibrational frequencies are also proved to be similar among the different 4f-electron configurations for the respective complexes.

Table 2 shows total energies (in Hartree), Ln–Cl bond lengths (in Å), Mulliken charges on Ln, and the expectation values of the square of the spin operator, $\langle S^2 \rangle$, calculated for several states of $CeCl_3$ and $PrCl_3$ by the UHF method with the addition of d-polarization function on Cl atoms. The comparison with corresponding values in Table 1 shows that the inclusion of polarization functions does not affect the order of energy levels of the corresponding states except the lowest state of $CeCl_3$ which changes from A'_2 to A''_2 (note their small energy difference); the Ln–Cl bond length becomes smaller by 0.02–0.03 Å, and the net charge on Ln increases by 0.1 in all cases.

The role of three orbitals, a'_1, a'_2, and a''_2, in the 4f-electron configurations are equivalent in the sense that they are non-degenerate orbitals. As shown in Table 1, the two states with 4f-electron configurations in which the occupation numbers of a'_1 and a'_2 orbitals are exchanged, have a similar energy in all $LnCl_3$. This result can be related to the spatial-distribution of f-orbitals. To illustrate this, top and side views of the 4f-related-MOs calculated for $GdCl_3$ (with seven 4f-electrons) are given in Fig. 1 (the sections corresponding to nodal planes are omitted). The a''_2 orbital stands orthogonal to the molecular plane and is localized almost completely on Ln, while the a'_1 and a'_2 orbitals both extend toward Cl atoms on the molecular plane; the difference between the a'_1 and a'_2 orbitals is the location of the nodal planes. No contributions are observed from the AOs of Cl in all the f-orbitals, indicating that the 4f-orbitals contract inside the atom. Fig. 2 shows variations of the expectation value of the spatial-extension of the respective 4f-orbitals in the molecular plane (x–y plane), the square root of $(\langle x^2 \rangle + \langle y^2 \rangle)$, in the series of lanthanide trichlorides ($CeCl_3$ to $YbCl_3$) calculated by the SA-CASSCF method. The expectation values, $\langle x^2 \rangle$ and $\langle y^2 \rangle$, were calculated by utilizing elements of the dipole moment matrix in terms of basis functions. As shown in Fig. 2, they all decrease with increasing atomic number. The extension of the respective orbitals coincides with those shown in

Table 1
Total energies, Ln–Cl bond lengths, and Mulliken charges on Ln calculated by the UHF method for all the possible non-degenerate 4f-electron configurations in the $LnCl_3$. The expectation values of the square of the spin operator, $\langle S^2 \rangle$, are also given

Ln	State	4f electron configuration	Total energy (Hartree)	Bond length (Å)	Mulliken charge	$\langle S^2 \rangle$
La	$^1A_1'$		−75.41210	2.697	1.56	
Ce	$^2A_2'$	$(a_2')^1$	−82.44913	2.644	1.51	0.75
	$^2A_2''$	$(a_2'')^1$	−82.44898	2.652	1.51	0.75
	$^2A_1'$	$(a_1')^1$	−82.44891	2.643	1.50	0.75
Pr	$^3A_1''$	$(a_2'')^1(a_2')^1$	−90.69396	2.632	1.48	2.01
	$^3A_2''$	$(a_2'')^1(a_1')^1$	−90.69365	2.632	1.48	2.01
	$^3A_2'$	$(e')^2$	−90.69149	2.634	1.48	2.01
	$^3A_2'$	$(e'')^2$	−90.66055	2.632	1.48	2.01
	$^3A_2'$	$(a_2')^1(a_1')^1$	−90.62860	2.624	1.48	2.02
Nd	$^4A_1'$	$(e')^2(a_2')^1$	−100.34406	2.618	1.45	3.76
	$^4A_2'$	$(e')^2(a_1')^1$	−100.34374	2.618	1.45	3.76
	$^4A_1''$	$(a_2'')^1(e'')^2$	−100.31968	2.617	1.46	3.76
	$^4A_1'$	$(e'')^2(a_2')^1$	−100.29209	2.615	1.45	3.76
	$^4A_2'$	$(e'')^2(a_1')^1$	−100.29175	2.615	1.45	3.76
	$^4A_1''$	$(a_2'')^1(e')^2$	−100.24858	2.618	1.45	3.76
	$^4A_1''$	$(a_2'')^1(a_2')^1(a_1')^1$	−100.09537	2.609	1.47	3.76
Pm	$^5A_2''$	$(a_2'')^1(e'')^2(a_2')^1$	−111.41872	2.606	1.43	6.01
	$^5A_1''$	$(a_2'')^1(e'')^2(a_1')^1$	−111.41839	2.606	1.43	6.01
	$^5A_1'$	$(e')^2(a_2')^1(a_1')^1$	−111.39107	2.604	1.42	6.01
	$^5A_2''$	$(a_2'')^1(e')^2(a_2')^1$	−111.36524	2.606	1.43	6.01
	$^5A_1''$	$(a_2'')^1(e')^2(a_1')^1$	−111.36489	2.606	1.43	6.01
	$^5A_1'$	$(e')^2(e'')^2$	−111.34703	2.606	1.43	6.01
	$^5A_1'$	$(e'')^2(a_2')^1(a_1')^1$	−111.31649	2.597	1.42	6.02
Sm	$^6A_2'$	$(e')^2(e'')^2(a_2')^1$	−123.97477	2.585	1.45	8.77
	$^6A_1'$	$(e')^2(e'')^2(a_1')^1$	−123.97418	2.585	1.44	8.77
	$^6A_2''$	$(a_2'')^1(e'')^2(a_2')^1(a_1')^1$	−123.96931	2.583	1.44	8.77
	$^6A_2''$	$(a_2'')^1(e')^2(a_2')^1(a_1')^1$	−123.93483	2.585	1.44	8.77
	$^6A_2''$	$(a_2'')^1(e')^2(e'')^2$	−123.90087	2.585	1.44	8.77
Eu	$^7A_1''$	$(a_2'')^1(e')^2(e'')^2(a_2')^1$	−138.15403	2.574	1.38	12.02
	$^7A_2''$	$(a_2'')^1(e')^2(e'')^2(a_1')^1$	−138.15343	2.574	1.38	12.02
	$^7A_2'$	$(e')^2(e'')^2(a_2')^1(a_1')^1$	−138.15004	2.574	1.38	12.03
Gd	$^8A_1''$	$(a_2'')^1(e')^2(e'')^2(a_2')^1(a_1')^1$	−154.03757	2.559	1.35	15.78
Tb	$^7A_2'$	$(a_2'')^2(e')^2(e'')^2(a_2')^1(a_1')^1$	−171.39196	2.549	1.32	12.02
	$^7A_1''$	$(a_2'')^1(e')^2(e'')^2(a_2')^1(a_1')^2$	−171.38875	2.547	1.32	12.02
	$^7A_2''$	$(a_2'')^1(e')^2(e'')^2(a_2')^2(a_1')^1$	−171.38852	2.547	1.32	12.02
Dy	$^6A_2'$	$(a_2'')^2(e')^2(e'')^2(a_2')^1(a_1')^2$	−190.56626	2.535	1.29	8.77
	$^6A_1'$	$(a_2'')^2(e')^2(e'')^2(a_2')^2(a_1')^1$	−190.56612	2.535	1.30	8.77
	$^6A_2''$	$(a_2'')^1(e')^4(e'')^2(a_2')^1(a_1')^1$	−190.56438	2.535	1.29	8.77
	$^6A_2''$	$(a_2'')^1(e')^2(e'')^4(a_2')^1(a_1')^1$	−190.52460	2.535	1.30	8.77
	$^6A_2''$	$(a_2'')^1(e')^2(e'')^2(a_2')^2(a_1')^2$	−190.47814	2.535	1.29	8.77

Table 1 (*Continued*)

Ln	State	4f electron configuration	Total energy (Hartree)	Bond length (Å)	Mulliken charge	$\langle S^2 \rangle$
Ho	$^5A_2''$	$(a_2'')^1(e')^4(e'')^2(a_2')^1(a_1')^2$	−211.66902	2.525	1.27	6.01
	$^5A_1''$	$(a_2'')^1(e')^4(e'')^2(a_2')^2(a_1')^1$	−211.66893	2.525	1.28	6.01
	$^5A_1'$	$(a_2'')^2(e')^2(e'')^4(a_2')^1(a_1')^1$	−211.63931	2.525	1.28	6.01
	$^5A_2''$	$(a_2'')^1(e')^2(e'')^4(a_2')^1(a_1')^2$	−211.60275	2.525	1.28	6.01
	$^5A_1''$	$(a_2'')^1(e')^2(e'')^4(a_2')^2(a_1')^1$	−211.60263	2.525	1.28	6.01
	$^5A_1'$	$(a_2'')^2(e')^2(e'')^2(a_2')^2(a_1')^2$	−211.58019	2.525	1.28	6.01
	$^5A_1'$	$(a_2'')^2(e')^4(e'')^2(a_2')^1(a_1')^1$	−211.55391	2.525	1.27	6.01
Er	$^4A_1'$	$(a_2'')^2(e')^2(e'')^4(a_2')^1(a_1')^2$	−234.70981	2.509	1.25	3.76
	$^4A_2'$	$(a_2'')^2(e')^2(e'')^4(a_2')^2(a_1')^1$	−234.70978	2.511	1.25	3.76
	$^4A_1''$	$(a_2'')^1(e')^4(e'')^2(a_2')^2(a_1')^2$	−234.67567	2.509	1.24	3.76
	$^4A_2''$	$(a_2'')^2(e')^4(e'')^2(a_2')^1(a_1')^2$	−234.64747	2.510	1.24	3.76
	$^4A_1'$	$(a_2'')^2(e')^4(e'')^2(a_2')^2(a_1')^1$	−234.64747	2.511	1.25	3.76
	$^4A_1''$	$(a_2'')^1(e')^4(e'')^4(a_2')^1(a_1')^1$	−234.62570	2.511	1.25	3.76
	$^4A_1''$	$(a_2'')^1(e')^2(e'')^4(a_2')^2(a_1')^2$	−234.58412	2.509	1.25	3.76
Tm	$^3A_1''$	$(a_2'')^1(e')^4(e'')^4(a_2')^1(a_1')^2$	−259.78355	2.502	1.23	2.00
	$^3A_2''$	$(a_2'')^1(e')^4(e'')^4(a_2')^2(a_1')^1$	−259.78353	2.502	1.23	2.00
	$^3A_2'$	$(a_2'')^2(e')^2(e'')^4(a_2')^2(a_1')^2$	−259.77356	2.502	1.23	2.00
	$^3A_2'$	$(a_2'')^2(e')^4(e'')^2(a_2')^2(a_1')^2$	−259.73612	2.502	1.23	2.00
	$^3A_2'$	$(a_2'')^2(e')^4(e'')^4(a_2')^1(a_1')^1$	−259.69620	2.502	1.23	2.00
Yb	$^2A_2'$	$(a_2'')^2(e')^4(e'')^4(a_2')^1(a_1')^2$	−286.99629	2.491	1.20	0.75
	$^2A_1'$	$(a_2'')^2(e')^4(e'')^4(a_2')^2(a_1')^1$	−286.99629	2.491	1.20	0.75
	$^2A_2''$	$(a_2'')^1(e')^4(e'')^4(a_2')^2(a_1')^2$	−286.98989	2.491	1.20	0.75
Lu	$^1A_1'$	$(a_2'')^2(e')^4(e'')^4(a_2')^2(a_1')^2$	−316.43617	2.480	1.17	

Fig. 1; the a_1' and a_2' orbitals show almost the same spatial-extension.

Fig. 3 shows the 4f-electron configuration for the lowest state of the respective $LnCl_3$ calculated by the UHF method. The order of energy levels of orbitals in the respective electron configurations coincides with the order of the α orbital energy. As is the usual case, the first seven

Table 2
Total energies, Ln–Cl bond lengths, and Mulliken charges on Ln calculated for several states of $CeCl_3$ and $PrCl_3$ by the UHF method with the addition of d-polarization function on Cl atoms. The expectation values of the square of the spin operator, $\langle S^2 \rangle$, are also given

Ln	State	4f electron configuration	Total energy (Hartree)	Bond length (Å)	Mulliken charge	$\langle S^2 \rangle$
Ce	A_2''	$(a_2'')^1$	−82.47153	2.624	1.59	0.75
	A_2'	$(a_2')^1$	−82.47146	2.619	1.58	0.75
	A_1'	$(a_1')^1$	−82.47124	2.619	1.57	0.75
Pr	A_1''	$(a_2'')^1(a_2')^1$	−90.71672	2.607	1.56	2.01
	A_2''	$(a_2'')^1(a_1')^1$	−90.71640	2.606	1.56	2.01
	A_2'	$(e')^2$	−90.71456	2.608	1.56	2.00
	A_2'	$(e'')^2$	−90.68356	2.604	1.56	2.01
	A_2'	$(a_2')^1(a_1')^1$	−90.65134	2.598	1.55	2.02

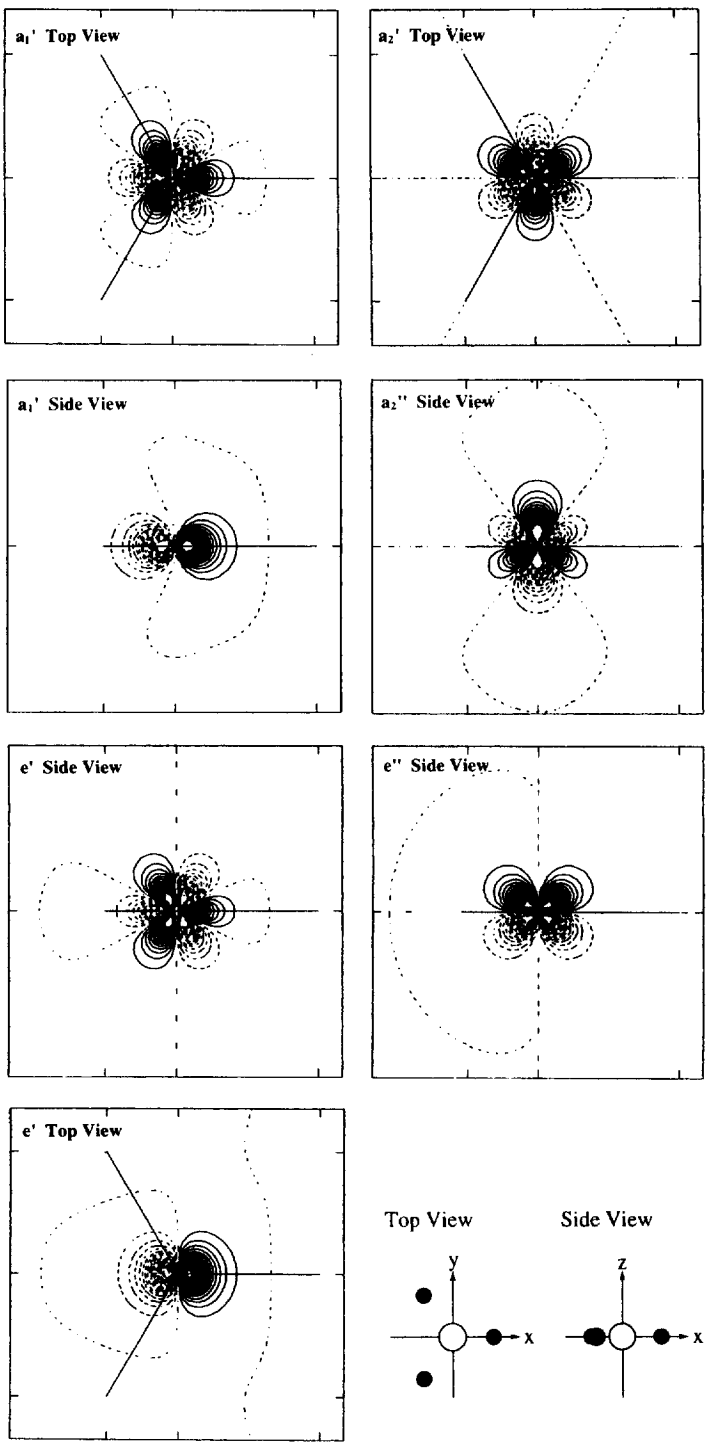

Fig. 1. Molecular orbitals related to 4f-orbitals calculated for $GdCl_3$, in which seven 4f-orbitals are all singly-occupied.

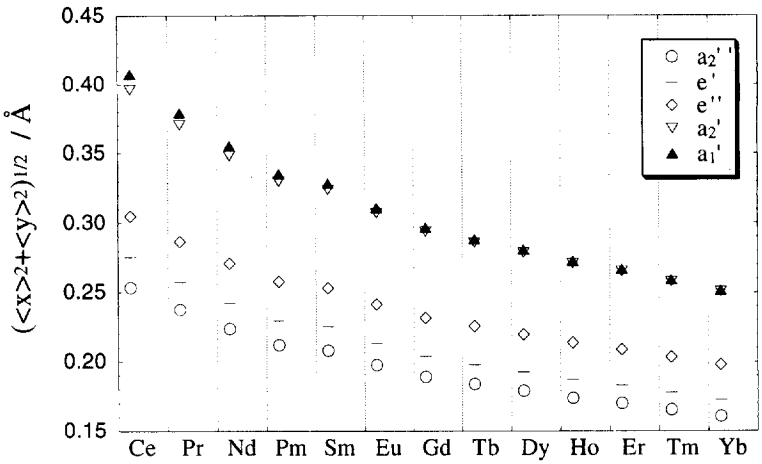

Fig. 2. Variations of the expectation value of the spatial-extension in the molecular plane (x–y plane) for the respective 4f-orbitals, the square root of ($\langle x^2 \rangle + \langle y^2 \rangle$), in the series of lanthanide trichlorides calculated by the SA-CASSCF method.

electrons occupy f-orbitals one by one from the lowest one. However, the second seven electrons occupy f-orbitals from the highest one down (see those of $TbCl_3$, $DyCl_3$, $HoCl_3$, $ErCl_3$, $TmCl_3$, and $YbCl_3$ in Fig. 3), which gives a strange configuration at first glance. This occupation mechanism can be understood in terms of electronic self-repulsion interactions: the 4f-orbitals contract toward the nucleus due to the strong cationic character of Ln^{3+}; the originally degenerate seven 4f-orbitals split out in the complex, $LnCl_3$, forming a nearly-degenerate orbital set; doubly-occupied 4f-orbitals become more unstable than singly-occupied 4f-orbitals due to the self-repulsion term between two electrons occupying the contracted same spatial orbital. The energy splitting between the lowest and the highest f-orbitals is 0.05, 2.84, 1.58, 1.29, 1.45, 1.60, 3.58, and 0.14 eV for $GdCl_3$, $TbCl_3$, $DyCl_3$, $HoCl_3$, $ErCl_3$, $TmCl_3$, $YbCl_3$, and $LuCl_3$, respectively. These small energy differences indicate that the 4f-orbitals form a nearly-degenerate system.

In the respective complexes, it is found that the electronic populations derived from UHF wavefunctions are almost similar to those derived from CASSCF wavefunctions. Analyses of the CASSCF atomic orbital populations show the valence-electron configurations of Ln to be $(4f)^n(5s)^2(5p)^6(5d)^1(6s)^{0.15-0.35}(6p)^{0.25-0.55}$ in $LnCl_3$ and $(4f)^n(5s)^2(5p)^6(5d)^{0.65}(6s)^{0.04-0.08}(6p)^{0.12-0.15}$ in LnF_3; the number of 4f-electrons increases one by one in the same way as the ground states of Ln^{3+} in both the complexes; the Ln–X bonds are dominated by charge-transfer but have a significant amount of covalent character that involves the 5d-orbitals (d_{xy}, $d_{x^2-y^2}$, d_{xz}, d_{yz}) on Ln where z-axis is taken orthogonal to the molecular plane. The covalent character of Ln–X bonds can be estimated from the deviation of net charges in Ln from +3, and from the amount of 5d, 6s, and 6p atomic orbital populations of Ln, P(5d), P(6s), and P(6p) (see descriptions in the first paragraph in this section). Fig. 4 shows variations of (a) Mulliken charges of Ln and (b) P(5d), P(6s), and P(6p) in $LnCl_3$ (solid marks) and in LnF_3 (open marks). As shown here, the covalent character is stronger in Ln–Cl than in Ln–F. The net charge of Ln in $LnCl_3$ decreases linearly from 1.6 to 1.2, with the increase of the atomic number, except for the net charge on Sm; Ln in LnF_3 has an almost constant net charge, 2.1–2.2. In $LnCl_3$, P(6s) and P(6p) increase linearly along the lanthanide series: $P(6s) = 0.0136n + 0.139$; $P(6p) = 0.0206n + 0.257$, where n represents the position number in the lanthanide series ($n_{La} = 0$); P(5d) shows a strange behavior at Sm, which appears also in variations of net charges in Fig. 4a. In LnF_3, almost constant values are observed in all P(5d), P(6s), and P(6p).

At the CASSCF level, all the complexes, $LnCl_3$

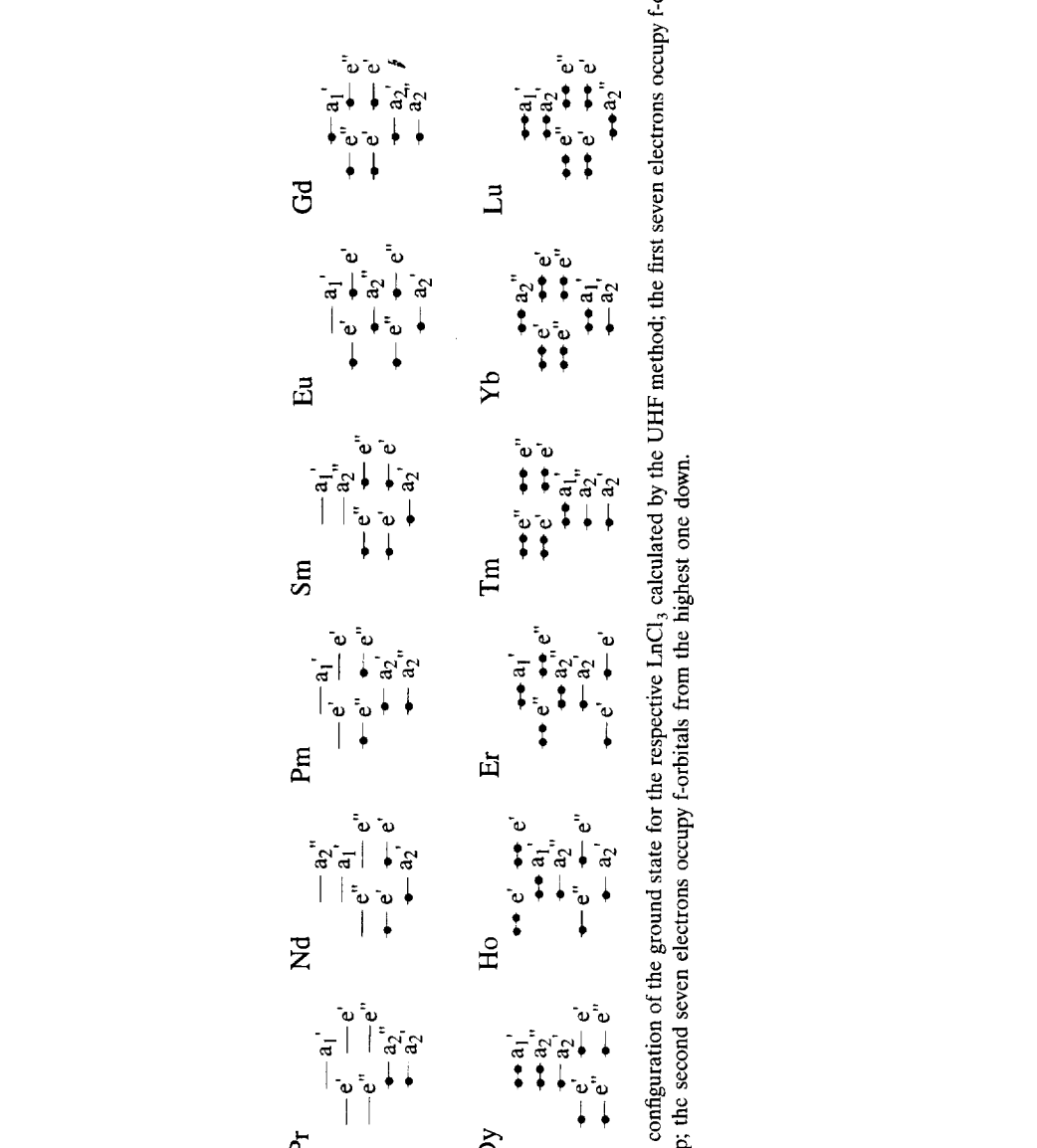

Fig. 3. The 4f-electron configuration of the ground state for the respective $LnCl_3$ calculated by the UHF method; the first seven electrons occupy f-orbitals one by one from the lowest one up; the second seven electrons occupy f-orbitals from the highest one down.

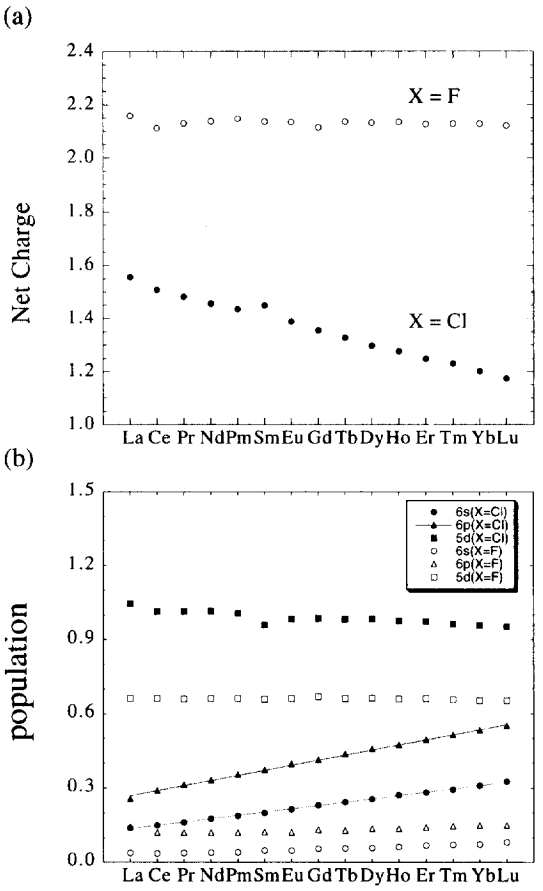

Fig. 4. Variations of (a) Mulliken charges of Ln and (b) 5d, 6s, and 6p atomic orbital populations in the ground state of $LnCl_3$ (open mark) and LnF_3 (solid mark) calculated by the CASSCF method.

and LnF_3, prove to have D_{3h} symmetry in their (stable) equilibrium structures through normal mode analyses. These results coincide with the results by Cundari et al. who carried out CASSCF geometrical optimizations for LnX_3 with C_{3v} symmetry constraint using a non-gradient energy minimizer [22]. In the complexes CeF_3, PrF_3, SmX_3 and TmX_3, the lowest state is calculated to be the degenerate state in D_{3h} symmetry, but they are proved to be stable relative to geometrical deformation, i.e. no Jahn–Teller effect is observed [30]. This indicates that the 4f-electron configurations have negligible influences on the molecular structure because 4f-electrons contract toward the nucleus.

Table 3
CASSCF natural orbital occupancies of principal configurational state functions and their weights for the ground state of $LnCl_3$[a]

Ln	Occupation					Symmetry	Weight (%)
	a_2''	e'	e''	a_2'	a_1'		
Ce	1	0	0	0	0	A_2''	100.0
Pr	0	2	0	0	0	A_2'	72.4
	0	0	2	0	0	A_2'	27.1
Nd	1	0	2	0	0	A_1''	38.5
	0	1	1	0	1	A_1''	15.7
	0	0	1	1	1	E''	15.2
	1	1	0	1	0	E''	29.8
Pm	0	1	1	1	1	A_2''	7.6
	1	2	0	1	0	A_2''	18.1
	1	0	2	1	0	A_2''	73.0
Sm	1	2	1	0	1	E'	49.0
	1	2	1	1	0	E'	51.0
Eu	1	2	2	1	0	A_1''	100.0
Gd	1	2	2	1	1	A_1''	100.0
Tb	2	2	2	1	1	A_2'	100.0
Dy	1	4	2	1	1	A_2''	74.9
	1	2	4	1	1	A_2''	24.7
Ho	1	3	3	1	2	A_1'	10.2
	1	3	3	2	1	A_1'	10.0
	2	2	2	2	2	A_1'	15.3
	2	4	2	1	1	A_1'	6.1
	2	2	4	1	1	A_1'	58.4
Er	2	3	3	1	2	A_1''	50.0
	2	3	3	2	1	A_1''	50.0
Tm	2	4	3	2	1	E''	50.0
	2	4	3	1	2	E''	50.0
Yb	2	4	4	1	2	A_2'	100.0

[a]Only configurations with weight loss of not less than 1.0% are shown.

Table 3 gives CASSCF natural orbital occupancies of principal configurational state functions and their weights for the ground state of $LnCl_3$,

where natural (4f) orbitals are represented by their symmetry representations (see Fig. 1). All configurations which contribute at least 1% to the wavefunction are included in this table. There is only one electronic configuration in the complexes, $CeCl_3$, $EuCl_3$, $GdCl_3$, $TbCl_3$, and $YbCl_3$, which have 1, 6, 7, 8, and 13 4f-electrons, respectively, so the CASSCF method coincides with the restricted open-shell Hartree–Fock (ROHF) method in these cases. In the other complexes, there is considerable configurational mixing. Note that, in $NdCl_3$, A_1'' and E″ electronic configurations contribute with almost equal weights (spatial-symmetry contamination). This is because we carried out CASSCF calculations with C_1 symmetry. Table 4 gives symmetry representations, active natural orbital occupation numbers, total energies, Ln–Cl bond lengths, and Mulliken charges on Ln for the ground state of $LnCl_3$ at the CASSCF level, with the Ln–Cl bond lengths estimated from gas-phase electron diffraction experiments [16]. The calculated Ln–Cl bond lengths are always longer than the experimental values, although only by 0.06–0.08 Å. Cundari et al. [22] reported the Ln–Cl bond length shorter than ours by 0.02–0.04 Å. Due to the near degeneracy, the order of energy levels of low-lying electronic states is rather sensitive to the computational level employed. Indeed, the lowest state at the CASSCF level is different from that determined by the UHF method in most cases (compare with Table 1). In $CeCl_3$, $EuCl_3$, $GdCl_3$, $TbCl_3$, and $YbCl_3$, the CASSCF energy becomes high relative to the UHF values because they coincide with the ROHF values. In all the complexes, the CASSCF geometric structures and Mulliken charges are almost the same as those at the UHF level, supporting that different 4f-electron configurations do not change the bonding mechanism of Ln–Cl.

Fig. 5 shows variations of Ln–X bond lengths in the lowest state of a series of $LnCl_3$ (open mark) and LnF_3 (solid mark) determined by the CASSCF method. The Ln–X bond length decreases linearly with the increase of the atomic number of Ln, except for the La–X bond length (no 4f-electron). This decrease can be related to the *lanthanide contraction*: the ion radii of lanthanide atoms decrease gradually with increasing atomic number because of the incompleteness of the screening effect of 4f-electrons. The Ln–Cl bond is always longer than the Ln–F bond by about 0.5 Å. Fig. 6 shows variations of CASSCF vibrational frequencies of six normal modes, four of which belong to doubly-degenerate pairs as shown there, calculated for the equilibrium structures in the ground state of (a) $LnCl_3$ and (b)

Table 4
CASSCF active natural orbital occupation numbers, total energies, Ln–Cl bond lengths, and Mulliken charges on Ln for the ground state of $LnCl_3$

Ln	State	Occupation number							Total energy	Bond length (Å)		Mulliken
		a_2''	e′	e′	e″	e″	a_2'	a_1'	(Hartree)	Cal.	Exp.[a]	charge
Ce	$^2A_2''$	1.00	0.00	0.00	0.00	0.00	0.00	0.00	−82.44837	2.647	2.58	1.51
Pr	$^3A_2'$	0.00	0.72	0.72	0.27	0.27	0.01	0.01	−90.70376	2.634	2.55	1.48
Nd	$^4A_1''(^4E'')$	0.69	0.01	0.46	0.54	0.54	0.45	0.31	−100.35951	2.618	2.54	1.46
Pm	$^5A_2''$	0.91	0.23	0.23	0.77	0.77	1.00	0.09	−111.43113	2.606	2.53	1.44
Sm	$^6E'$	1.00	1.00	1.00	0.49	0.51	0.51	0.49	−123.97940	2.585	2.52	1.45
Eu	$^7A_1''$	1.00	1.00	1.00	1.00	1.00	1.00	0.00	−138.13997	2.575	2.50	1.39
Gd	$^8A_1''$	1.00	1.00	1.00	1.00	1.00	1.00	1.00	−154.01907	2.559	2.49	1.36
Tb	$^7A_2'$	2.00	1.00	1.00	1.00	1.00	1.00	1.00	−171.37695	2.549	2.48	1.33
Dy	$^6A_2''$	1.00	1.75	1.75	1.25	1.25	1.00	1.00	−190.57067	2.535	2.47	1.30
Ho	$^5A_1'$	1.80	1.16	1.16	1.68	1.68	1.25	1.25	−211.68504	2.525	2.46	1.28
Er	$^4A_1''$	2.00	1.50	1.50	1.50	1.50	1.50	1.50	−234.73048	2.511	2.45	1.25
Tm	$^3E''$	2.00	2.00	2.00	1.50	1.50	1.50	1.50	−259.79915	2.502	2.44	1.23
Yb	$^2A_2'$	2.00	2.00	2.00	2.00	2.00	1.00	2.00	−286.99520	2.491	2.43	1.20

[a] See ref. [16].

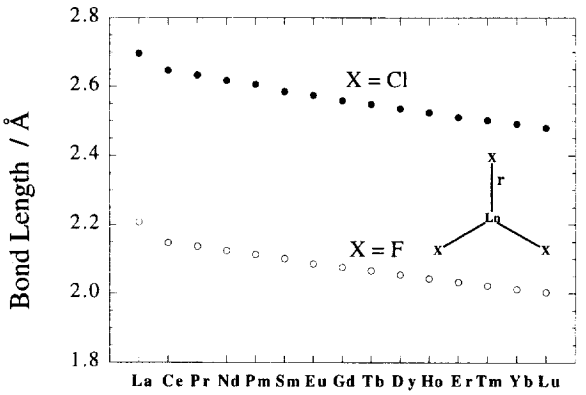

Fig. 5. Variations of Ln–X bond lengths in the ground state of a series of $LnCl_3$ (open mark) and LnF_3 (solid mark) calculated by the CASSCF method.

LnF_3. The stretching vibrational modes with high frequency show an almost monotonic (increasing) variation with increasing atomic number, which corresponds to the decrease of Ln–X bond lengths: the short bond length indicates a strong chemical bonding. The mode with the highest frequency is E′ in $LnCl_3$, while it is A'_1 in LnF_3. On the other hand, the bending vibrational modes with low frequency show a not-so-monotonous behavior. This may be related to the fact that Ln–X bond length does not so change due to bending motions. The small frequency of the out-of-plane mode suggests that they are floppy molecules relative to the out-of-plane motion.

3.2. Nearly degenerate states of $LnCl_3$

The near-degeneracy of electronic states of LnX_3 is caused by plural different 4f-electron-configurations. As described in the previous section, the number of 4f-electrons in the lowest states of LnX_3 coincides with that in the ground states of Ln^{3+}. Thus, without the inclusion of spin-orbit coupling, the number of nearly-degenerate low-lying states of LnX_3 should coincide with the number of the spatial-degeneracy of the ground states of Ln^{3+}, $(2L+1)$ (7 for Ce^{3+}, Eu^{3+}, Tb^{3+}, Yb^{3+}; 11 for Pr^{3+}, Sm^{3+}, Dy^{3+}, Tm^{3+}; 13 for Nd^{3+}, Pm^{3+}, Ho^{3+}, Er^{3+}), related to the number of electrons or holes in 4f-orbitals.

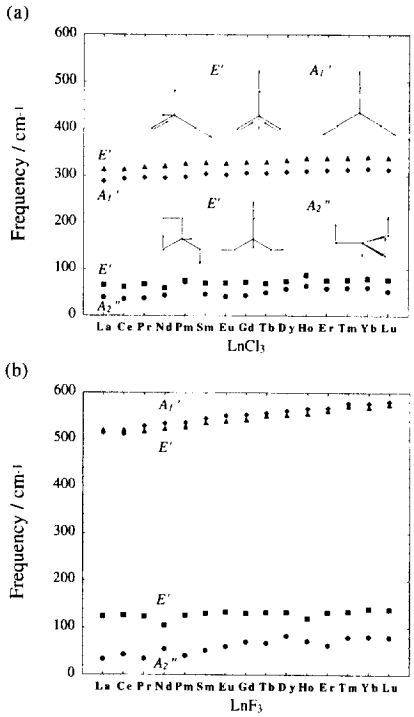

Fig. 6. Variations of CASSCF vibrational frequencies of six normal modes in the ground state of (a) $LnCl_3$ and (b) LnF_3.

Fig. 7 shows energies of those nearly-degenerate states of $LnCl_3$ (Ln = Ce, Pr, Nd, Pm, Sm, Eu, Tb, Dy, Ho, Er, Tm, Yb) relative to that of the respective lowest states, calculated by the SA-CASSCF method. The energy splittings between the lowest and highest states are very small (2–14 kJ/mol). The lowest states at the SA-CASSCF level coincide with those at the (state-specific) CASSCF level (compare Fig. 7 with Table 4). In these calculations, the spin-orbit coupling has not been taken into account explicitly although Cundari's RECP employed here was determined including Darwin, mass-velocity, and spin-orbit terms [3].

First, we would pick up several features of spin-orbit-uncoupled low-lying states given in Fig. 7. According to the number of nearly-degenerate states (= 7, 11, or 13), the numbers of the respective non-degenerate (A'_1, A''_1, A'_2, A''_2) and degenerate (E′, E″) states can be specified. The splitting pattern of nearly-degenerate states in the first six complexes (group 1: $CeCl_3$ to $EuCl_3$) is similar to

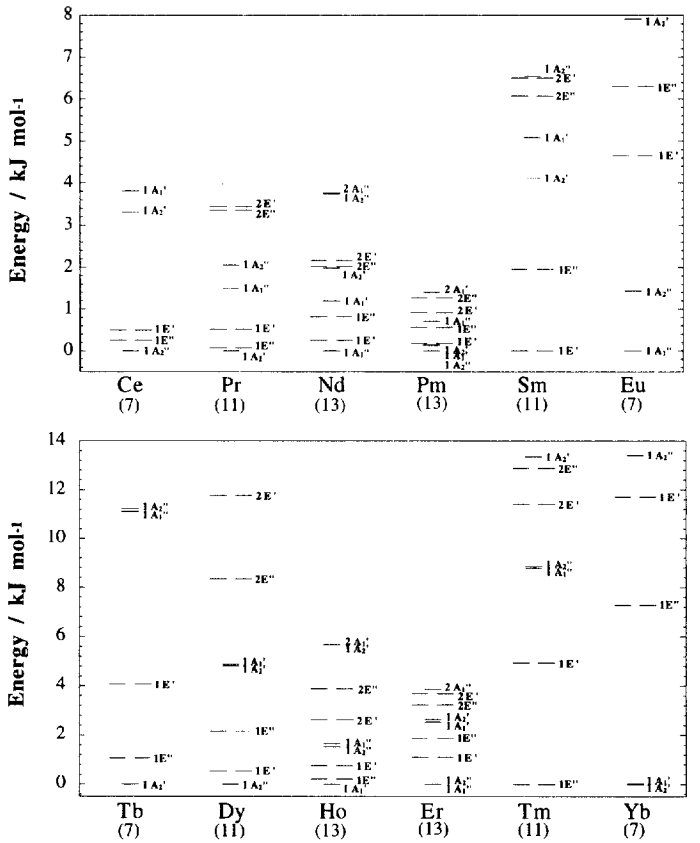

Fig. 7. Energy levels of the nearly-degenerate low-lying states calculated by the SA-CASSCF method, including only 4f-orbitals as the active space, averaging over the number of the degeneracy of the ground states of Ln^{3+} (given in the parentheses) for the respective $LnCl_3$. The energies are given relative to that of the respective lowest states.

that in the latter six complexes (group 2: $TbCl_3$ to $YbCl_3$), respectively, although the energy splitting between the lowest and highest ones becomes larger in group 2. Note that symmetry representations of electronic states of the complex in group 1 do not coincide, in most cases, with those of the corresponding complex in group 2. This is because of the symmetry representation of the half-filled 4f-electron configuration, A''_1 ($GdCl_3$): the direct product of A''_1 and the representation of electronic state of the complex in group 1 becomes the representation of electronic state of the corresponding complex in group 2. On the other hand, symmetry representations of a set of nearly-degenerate states of the compound with n electrons in 4f-orbitals coincide with those of the compound with n holes in 4f-orbitals (e.g. $CeCl_3$ and $YbCl_3$) although the order of the respective states in the former complex is basically opposite to that in the latter complex. The energy splitting pattern in LnF_3 is very similar to those in $LnCl_3$, although the magnitude of energy splitting is slightly larger (8–24 kJ/mol) because of stronger interaction from ligands.

In order to check effects from the excited states of different spin multiplicity, we also determined the CASSCF wavefunction and energy for the lowest (open-shell) singlet state of $PrCl_3$ (the ground state of $PrCl_3$ is triplet), with two electrons scattered over seven 4f-orbitals in the active space. The lowest singlet state was calculated to be $^1A'_1$, with natural orbital occupancies as

$$(a''_2)^{0.54}(e')^{0.01}(e')^{0.01}(e'')^{0.62}(e'')^{0.62}$$
$$(a'_2)^{0.09}(a'_1)^{0.09}, \quad (3)$$

and its energy was calculated as 65.4 kJ/mol above the ($^3A'_2$) lowest state (atomic orbital populations are almost the same as those in the triplet states). See Table 4 for natural orbital occupancies in $^3A'_2$. As shown in Fig. 7, 11 low-lying triplet states of $PrCl_3$ stay within the range of 3.5 kJ/mol, so the spin-orbit effects from the $^1A'_1$ state may be negligible within a context of zero L–S coupling.

Next, we proceed to evaluations of the energy splittings of low-lying *spin-coupled* states. In the present calculations, spin-orbit-coupling effects are included by employing a scheme of L–S coupling [4], in which the (L, S) state with $(2L+1)(2S+1)$-fold degeneracy is replaced by plural J-states with $(2J+1)$-fold degeneracy where J ($=L-S,\ldots,L+S$) is a quantum number of the total electronic angular momentum. Note that $L \geq S$ in a series of Ln^{3+} but Gd^{3+}. If the second order spin-orbit interactions are negligibly small, the energy for J-state can be expressed as,

$$E(J) = E_0 + \frac{\lambda}{2}[J(J+1) - L(L+1) - S(S+1)], \quad (4)$$

where E_0 is an energy for the (L, S) state (zero L–S coupling), and λ is a parameter depending on each parent LS term. This energy expression results in the Lande interval rule [31] as

$$E(J) - E(J-1) = \lambda J. \quad (5)$$

The parameter λ can be related to a spin-orbit coupling constant (SOC) ζ as [5,6]

$$\lambda = \begin{cases} \dfrac{\zeta}{n} & (1 \leq n \leq 6) \\ \dfrac{-\zeta}{14-n} & (8 \leq n \leq 13). \end{cases} \quad (6)$$

Table 5 gives SOCs for ground states of Ln^{3+} derived from experiments [32]. By utilizing these constants with Eqs. (4) and (6), we calculated energy levels of J-states of the ground states of Ln^{3+}. Fig. 8 shows those energy levels relative to the lowest state and the respective degeneracy, $(2J+1)$. The degeneracy of the respective states increases upward for n (number of 4f-electrons) < 7, while the degeneracy increases downward for $n > 7$: this is because of signs of λ defined in Eq. (6). The energy splittings in Fig. 8 are much larger than those in $LnCl_3$ with zero L–S coupling given in Fig. 7. The magnitude of the energy splitting in $YbCl_3$ (with one hole in 4f-orbitals) is especially larger than others.

The occupation of 4f-orbitals in the low-lying states of $LnCl_3$ is similar to that in the ground states of Ln^{3+}, indicating that 4f-orbitals in $LnCl_3$ are not distorted significantly from the atomic ion orbitals. Thus, it is safe to estimate the spin-orbit coupling constant for $LnCl_3$ from the atomic splittings. In order to estimate the energy splittings in $LnCl_3$ including spin-orbit coupling effects, we first introduced three kinds of basis sets, $\mathbf{J} = \{|J, M_J\rangle\}$, $\mathbf{L} = \{|L, M_L, S, M_S\rangle\}$, and $\mathbf{D} = \{|\psi_{D3h,i}\rangle\}$, where M_L and M_S denote quantum numbers for z-components of total-orbital-angular-momentum and total-spin-angular-momentum, respectively, and $|\psi_{D3h,i}\rangle$ indicates the ith electronic configuration written in terms of molecular orbitals labeled by irreducible representations of D_{3h} symmetry (a''_2, e', e', e'', e'', a'_2, a'_1) given in Fig. 1. $|J, M_J\rangle$ corresponds to simultaneous eigenfunctions of the total electronic an-

Table 5
Spin-orbit coupling constants [32] (in kJ/mol) for ground states of Ln^{3+}. The value for Pm^{3+} was estimated by fitting SOCs for Ce^{3+}–Eu^{3+} to a linear expression

	Ce	Pr	Nd	Pm	Sm	Eu	Tb	Dy	Ho	Er	Tm	Yb
SOC	7.66	8.97	10.77	(12.58)	14.12	16.27	19.38	21.77	24.88	29.55	32.90	35.29

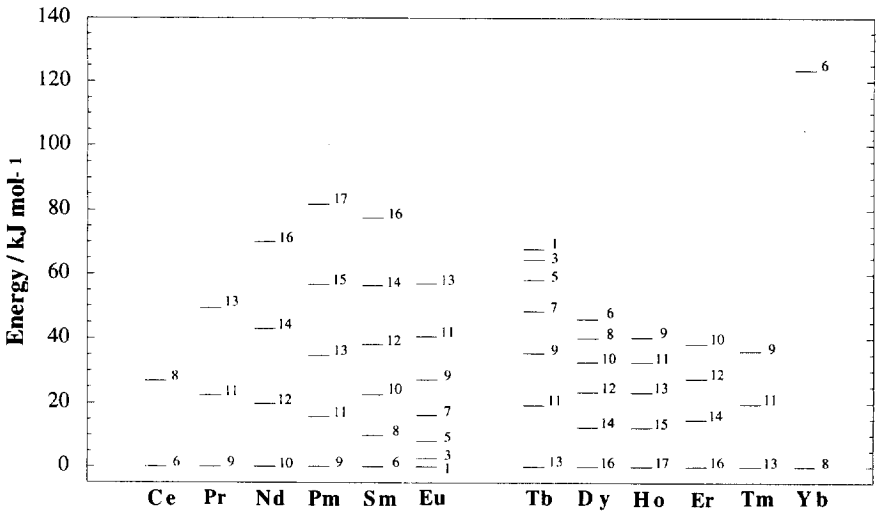

Fig. 8. Energy levels of J-states of the ground states of Ln^{3+} relative to the lowest state, with the respective degeneracy, calculated based on Eq. (4) and SOCs in Table 1.

gular momentum and its z-component, while $|L, M_L, S, M_S\rangle$ corresponds to simultaneous eigenfunctions of the total-orbital-angular-momentum, total-spin-angular-momentum, and their z-components. In Appendix A, the relations between **J** and **L**, and the relations between **L** and **D** are given for the case with one 4f-electron. It is also interesting to see the relations between $\mathbf{J} = \{|J, M_J\rangle\}$ and $\mathbf{D} = \{|\psi_{D3h,i}\rangle\}$. By substituting Eqs. (A16) and (A22) into Eqs. (A2) and (A9), for example, the functions $|J, M_J\rangle = |7/2, 5/2\rangle$ and $|5/2, 5/2\rangle$ can be expressed as,

$$\left|\frac{7}{2},\frac{5}{2}\right\rangle = \sqrt{\frac{6}{7}}\,\frac{e'' + ie''}{\sqrt{2}} + \sqrt{\frac{1}{7}}\,\frac{\bar{a}'_2 + i\bar{a}'_1}{\sqrt{2}}, \qquad (7)$$

$$\left|\frac{5}{2},\frac{5}{2}\right\rangle = \sqrt{\frac{1}{7}}\,\frac{e'' + ie''}{\sqrt{2}} - \sqrt{\frac{6}{7}}\,\frac{\bar{a}'_2 + i\bar{a}'_1}{\sqrt{2}}. \qquad (8)$$

The energies of the respective states are largely different from each other shown in Fig. 8, indicating that e″, $\bar{a}'_2$ and $\bar{a}'_1$ states in D_{3h} symmetry can mix in with each other. Similarly, it is derived that different symmetry representations of D_{3h} symmetry mix in with each other within three groups, i.e. {a''_2, e′}, {e″, e′}, and {a'_1, a'_2, e″}, respectively. By substituting Eqs. (A21) and (A27) into Eq. (A7), $|J, M_J\rangle = |7/2, -5/2\rangle$ can be expressed as,

$$\left|\frac{7}{2},-\frac{5}{2}\right\rangle = \sqrt{\frac{6}{7}}\,\frac{\bar{e}'' - i\bar{e}''}{\sqrt{2}} + \sqrt{\frac{1}{7}}\,\frac{a'_2 - ia'_1}{\sqrt{2}}. \qquad (9)$$

The comparison of Eqs. (7) and (9) indicates that, in the twofold degenerate pair, there is a complex–conjugate relation in the respective components although the roles of α and β spin functions are exchanged.

Among the series of lanthanide complexes, $CeCl_3$ (one electron) and $YbCl_3$ (one hole) are the easiest ones to evaluate the energy splittings. In Ce^{3+} and Yb^{3+} ($L = 3$ and $S = 1/2$), the ground states are 14-fold degenerate under zero L–S coupling. Due to the interaction with three Cl atoms, these states split into seven doubly-degenerate states in $CeCl_3$ and $YbCl_3$ within 4 and 14 kJ/mol, respectively (the degeneracy due to the spin multiplicity remains with zero L–S coupling), while the L–S coupling splits the 14-fold states of Ce^{3+} and Yb^{3+} into eightfold- ($J = 7/2$: $^2F_{7/2}$) and sixfold- ($J = 5/2$: $^2F_{5/2}$) degenerate states with energy separations of 26.8 and 123.5 kJ/mol, respectively. Fig. 9 shows energy levels of the 14 spin-orbit coupled states for (a) $CeCl_3$ and

(b) $YbCl_3$ calculated through the diagonalization of $\mathbf{H}^{tot}$ defined in Eq. (A29) in Appendix B, with the dotted lines denoting spin-orbit splittings for the ground states of Ce^{3+} and Yb^{3+}. Magnitudes of the energy separations indicate that the states first split into two sets due to the spin-orbit coupling with roughly the same magnitude as the corresponding energy splitting shown in Fig. 8, then, in the respective sets, the states further split in smaller magnitudes due to the interaction from Cl atoms. Also, Fig. 9 indicates that the respective states can be approximately expressed by the eigenstate of the total electronic angular momentum and its z-component, $|J, M_J\rangle$ (contributions from the other states are less than 0.2% at most), and there remains degeneracy between $|J, M_J\rangle$ and $|J, -M_J\rangle$; in other words, the L–S coupling separates the states of different value of J, then the ligand field from Cl-atoms in D_{3h} symmetry separates the states of different magnitude of $|M_J|$. As shown in Fig. 9, as $|M_J|$ increases (decreases), the energy increases in $CeCl_3$ ($YbCl_3$). The ground states of $CeCl_3$ are $|J, M_J\rangle = |5/2, \pm 1/2\rangle$, with $|5/2, \pm 3/2\rangle$ lying just 0.04 kJ/mol higher in energy. The transformation of the representation from **J** to **D** indicates the symmetry representation of the ground states of $CeCl_3$ to be $\{a''_2, e'\}$ in D_{3h} symmetry.

To show general features of spin-orbit coupled low-lying states for the series of lanthanide complexes, we give here the results of spin-orbit calculations for (a) $PrCl_3$ (two electrons), (b) $SmCl_3$ (five electrons), (c) $EuCl_3$ (six electrons), and (d) $TbCl_3$ (six holes) in Fig. 10. As is the case of $CeCl_3$ and $YbCl_3$ discussed above, the mechanism of energy splittings can be understood as the combination of spin-orbit splittings and the splittings due to interactions from Cl atoms. In $SmCl_3$ (odd number of 4f-electrons), the respective states can be specified by $|J, M_J\rangle$, and there remains the degeneracy between $|J, M_J\rangle$ and $|J, -M_J\rangle$ like $CeCl_3$ and $YbCl_3$; as $|M_J|$ increases within a set of states with a given J, the energy decreases. On the other hand, the degeneracy of the states, $|J, 3\rangle$ and $|J, -3\rangle$, breaks in the complexes with even number of 4f-electrons ($PrCl_3$, $EuCl_3$, $TbCl_3$), resulting in $(|J, 3\rangle \pm |J, -3\rangle)/2^{1/2}$. Note that, in such systems, there is always a non-degenerate state $|J, 0\rangle$. In $PrCl_3$, the highest states in the manifold of the lowest triplet states are $|6, 5\rangle$

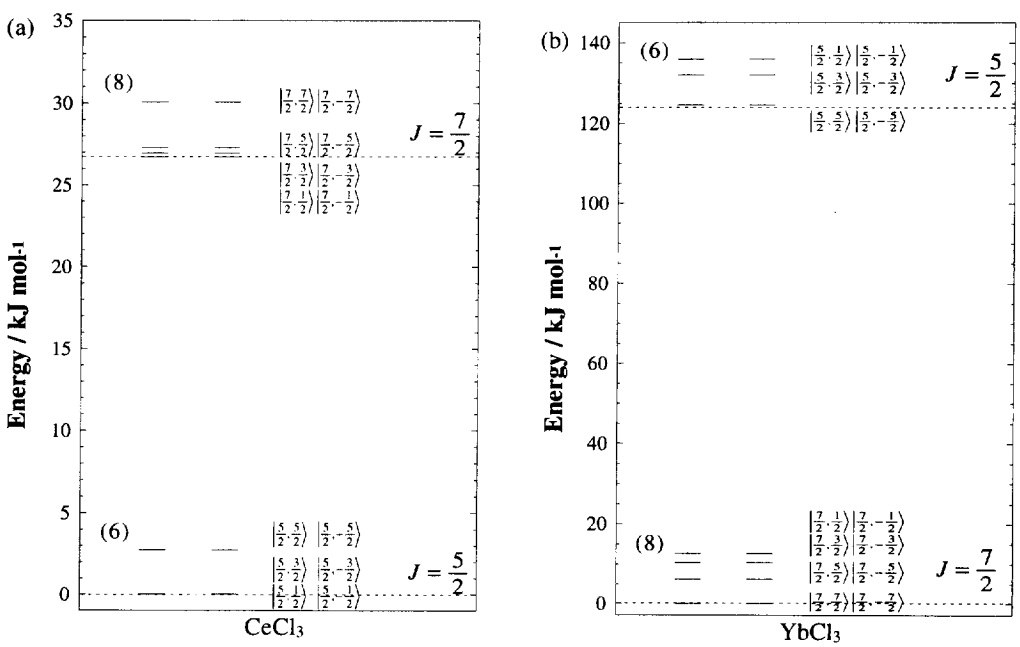

Fig. 9. Energy levels of spin-orbit coupled states: (a) $CeCl_3$; (b) $YbCl_3$.

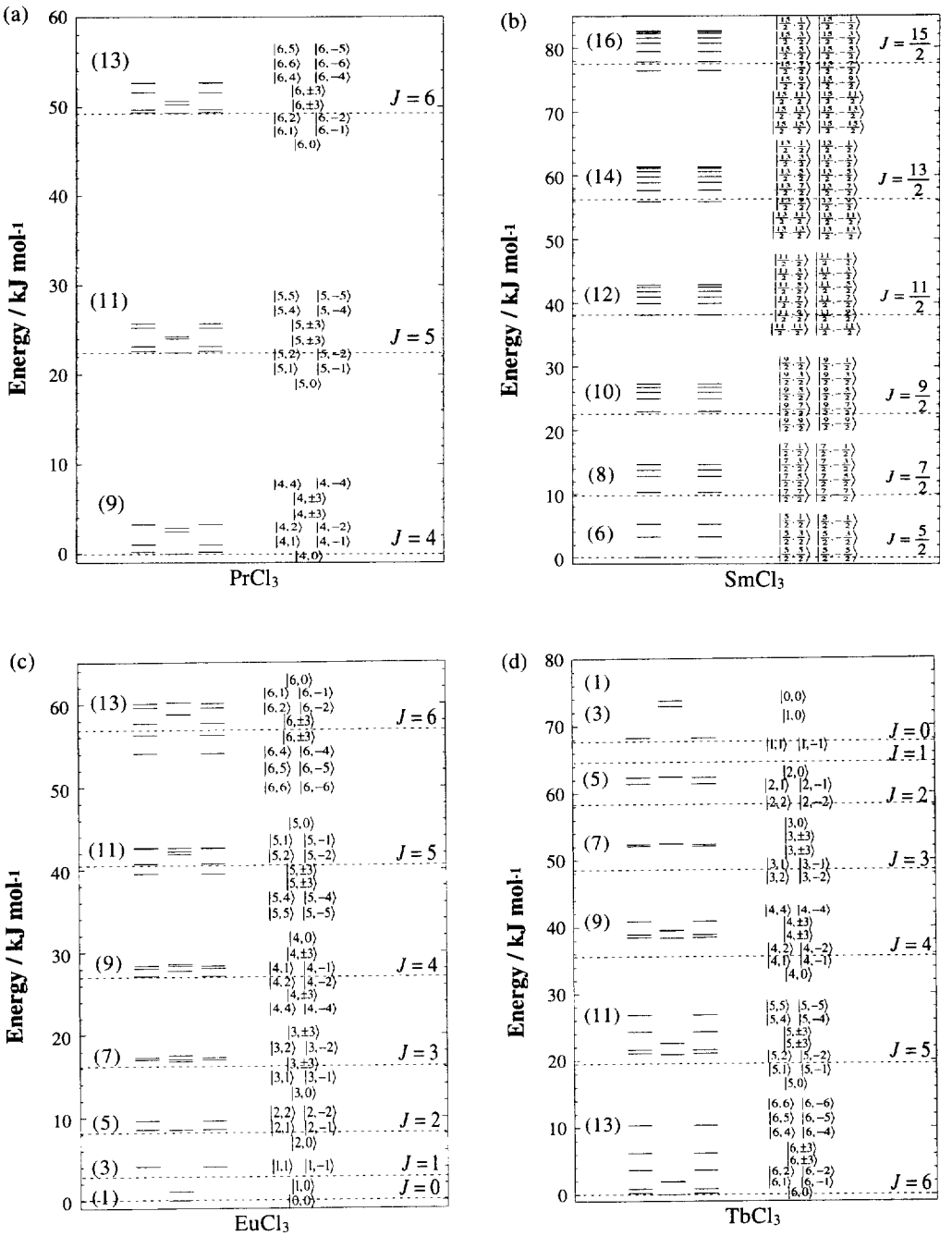

Fig. 10. Energy levels of spin-orbit coupled states: (a) $PrCl_3$; (b) $SmCl_3$; (c) $EuCl_3$; (d) $TbCl_3$.

and $|6, -5\rangle$, of which energy was calculated as 52.7 kJ/mol relative to the lowest state $|4, 0\rangle$. According to Eq. (4), the lowest state $|4, 0\rangle$ has been stabilized due to L–S coupling by about 27 kJ/mol. Recall that the energy of the lowest singlet state of $PrCl_3$ was calculated as 65.4 kJ/mol above the lowest triplet state under zero L–S coupling. These results suggest a slight necessity to include the second-order spin-orbit interactions from this singlet excited state for the quantitative evaluation of energy levels of the triplet states with $J = 6$ (their energy separation is calculated as about 40 kJ/mol).

4. Summary and conclusions

We investigated the electronic and geometrical structures of the series of lanthanide trihalides by the UHF and CASSCF methods with the employment of the RECP. First, the most stable spin symmetry is determined for the respective complexes, which coincides with the ground states of Ln^{3+}. In the LnX_3, the number of 4f-electrons increases by one with each unit increase of the atomic number; the Ln–X bonds are dominated by charge-transfer but have a significant amount of covalent character that involves the 5d-orbitals on Ln. In all the complexes, the planar structure (D_{3h} symmetry) proves to be stable through the normal mode analyses at the CASSCF levels. In the UHF method, equilibrium structures were located for all the possible non-degenerate 4f-electron configurations for the respective complexes. The results show that the Ln–Cl bond length and net charge on Ln are independent of 4f-electron configuration. The Ln–Cl bond length, net charge, and vibrational frequencies show monotonic variation along the lanthanide series, which corresponds to the *lanthanide contraction.*

It is observed that, along the lanthanide series, the first seven electrons occupy 4f-orbitals one by one from the lowest one up, while the second seven electrons occupy 4f-orbitals from the highest one down, as shown in Fig. 3. This occupation mechanism is explained as follows: the 4f-orbitals contract toward the nucleus due to the strong cationic character of Ln^{3+}; the originally degenerate seven 4f-orbitals split out in the complex, $LnCl_3$, forming a nearly-degenerate orbital set; doubly-occupied 4f-orbitals become more unstable than singly-occupied 4f-orbitals due to the self-repulsion term between two electrons occupying the same spatial contracted orbital.

SA-CASSCF and the following spin-orbit calculations clarify several features in energy splittings of nearly-degenerate low-lying states for the respective complexes: the spin-orbit coupling split the nearly-degenerate low-lying states of $LnCl_3$ into several states with the respective J in the order of ~ 130 kJ/mol, then the interaction from Cl atoms split the respective J-states into several states with the respective $|M_J|$ in the order of ~ 15 kJ/mol.

Acknowledgements

We are grateful to Dr. Nikita Matsunaga, Dr. Shiro Koseki, and Dr. Satoshi Yabushita for helpful suggestions on calculations of the spin-orbit splittings of the ground states of LnX_3. The present work was supported in part by a Grant-in-Aid for Scientific Research on Priority Areas 'New Development of Rare Earth Complexes' No. 08232218 from the Ministry of Education, Science and Culture.

Appendix A

The transformation among three basis sets, $|J, M_J\rangle$, $|L, M_L, S, M_S\rangle$, and $|\psi_{D3h,i}\rangle$, is demonstrated for the case with one 4f-electron; $L = 3$; $S = 1/2$; $J = 7/2$ (eightfold degenerate), $5/2$ (sixfold degenerate)). Basis functions, $|J, M_J\rangle$, are expressed in terms of $|L, M_L, S, M_S\rangle$ as,

$$\left|\frac{7}{2},\frac{7}{2}\right\rangle = \left|3,3,\frac{1}{2},\frac{1}{2}\right\rangle, \tag{A1}$$

$$\left|\frac{7}{2},\frac{5}{2}\right\rangle = \sqrt{\frac{6}{7}}\left|3,2,\frac{1}{2},\frac{1}{2}\right\rangle + \sqrt{\frac{1}{7}}\left|3,3,\frac{1}{2},-\frac{1}{2}\right\rangle, \tag{A2}$$

$$\left|\frac{7}{2},\frac{3}{2}\right\rangle = \sqrt{\frac{5}{7}}\left|3,1,\frac{1}{2},\frac{1}{2}\right\rangle + \sqrt{\frac{2}{7}}\left|3,2,\frac{1}{2},-\frac{1}{2}\right\rangle, \tag{A3}$$

$$\left|\frac{7}{2},\frac{1}{2}\right\rangle=\sqrt{\frac{4}{7}}\left|3,0,\frac{1}{2},\frac{1}{2}\right\rangle+\sqrt{\frac{3}{7}}\left|3,1,\frac{1}{2},-\frac{1}{2}\right\rangle, \tag{A4}$$

$$\left|\frac{7}{2},-\frac{1}{2}\right\rangle=\sqrt{\frac{3}{7}}\left|3,-1,\frac{1}{2},\frac{1}{2}\right\rangle+\sqrt{\frac{4}{7}}\left|3,0,\frac{1}{2},-\frac{1}{2}\right\rangle, \tag{A5}$$

$$\left|\frac{7}{2},-\frac{3}{2}\right\rangle=\sqrt{\frac{2}{7}}\left|3,-2,\frac{1}{2},\frac{1}{2}\right\rangle+\sqrt{\frac{5}{7}}\left|3,-1,\frac{1}{2},-\frac{1}{2}\right\rangle, \tag{A6}$$

$$\left|\frac{7}{2},-\frac{5}{2}\right\rangle=\sqrt{\frac{1}{7}}\left|3,-3,\frac{1}{2},\frac{1}{2}\right\rangle+\sqrt{\frac{6}{7}}\left|3,-2,\frac{1}{2},-\frac{1}{2}\right\rangle, \tag{A7}$$

$$\left|\frac{7}{2},-\frac{7}{2}\right|=\left|3,-3,\frac{1}{2},-\frac{1}{2}\right\rangle, \tag{A8}$$

$$\left|\frac{5}{2},\frac{5}{2}\right\rangle=\sqrt{\frac{1}{7}}\left|3,2,\frac{1}{2},\frac{1}{2}\right\rangle-\sqrt{\frac{6}{7}}\left|3,3,\frac{1}{2},-\frac{1}{2}\right\rangle, \tag{A9}$$

$$\left|\frac{5}{2},\frac{3}{2}\right\rangle=\sqrt{\frac{2}{7}}\left|3,1,\frac{1}{2},\frac{1}{2}\right\rangle-\sqrt{\frac{5}{7}}\left|3,2,\frac{1}{2},-\frac{1}{2}\right\rangle, \tag{A10}$$

$$\left|\frac{5}{2},\frac{1}{2}\right\rangle=\sqrt{\frac{3}{7}}\left|3,0,\frac{1}{2},\frac{1}{2}\right\rangle-\sqrt{\frac{4}{7}}\left|3,1,\frac{1}{2},-\frac{1}{2}\right\rangle, \tag{A11}$$

$$\left|\frac{5}{2},-\frac{1}{2}\right\rangle=\sqrt{\frac{4}{7}}\left|3,-1,\frac{1}{2},\frac{1}{2}\right\rangle-\sqrt{\frac{3}{7}}\left|3,0,\frac{1}{2},-\frac{1}{2}\right\rangle, \tag{A12}$$

$$\left|\frac{5}{2},-\frac{3}{2}\right\rangle=\sqrt{\frac{5}{7}}\left|3,-2,\frac{1}{2},\frac{1}{2}\right\rangle-\sqrt{\frac{2}{7}}\left|3,-1,\frac{1}{2},-\frac{1}{2}\right\rangle, \tag{A13}$$

$$\left|\frac{5}{2},-\frac{5}{2}\right\rangle=\sqrt{\frac{6}{7}}\left|3,-3,\frac{1}{2},\frac{1}{2}\right\rangle-\sqrt{\frac{1}{7}}\left|3,-2,\frac{1}{2},-\frac{1}{2}\right\rangle. \tag{A14}$$

The correspondence between $|L, M_L, S, M_S\rangle$ and $|\psi_{\mathrm{D3h},i}\rangle$ can be written as,

$$\left|3,3,\frac{1}{2},\frac{1}{2}\right\rangle=\frac{a'_2+ia'_1}{\sqrt{2}}, \tag{A15}$$

$$\left|3,2,\frac{1}{2},\frac{1}{2}\right\rangle=\frac{e''+ie''}{\sqrt{2}}, \tag{A16}$$

$$\left|3,1,\frac{1}{2},\frac{1}{2}\right\rangle=\frac{e'+ie'}{\sqrt{2}}, \tag{A17}$$

$$\left|3,0,\frac{1}{2},\frac{1}{2}\right\rangle=a''_2, \tag{A18}$$

$$\left|3,-1,\frac{1}{2},\frac{1}{2}\right\rangle=\frac{e'-ie'}{\sqrt{2}}, \tag{A19}$$

$$\left|3,-2,\frac{1}{2},\frac{1}{2}\right\rangle=\frac{e''-ie''}{\sqrt{2}}, \tag{A20}$$

$$\left|3,-3,\frac{1}{2},\frac{1}{2}\right\rangle=\frac{a'_2-ia'_1}{\sqrt{2}}, \tag{A21}$$

$$\left|3,3,\frac{1}{2},-\frac{1}{2}\right\rangle=\frac{\bar{a}'_2+i\bar{a}'_1}{\sqrt{2}}, \tag{A22}$$

$$\left|3,2,\frac{1}{2},-\frac{1}{2}\right\rangle=\frac{\bar{e}''+i\bar{e}''}{\sqrt{2}}, \tag{A23}$$

$$\left|3,1,\frac{1}{2},-\frac{1}{2}\right\rangle=\frac{\bar{e}'+i\bar{e}'}{\sqrt{2}}, \tag{A24}$$

$$\left|3,0,\frac{1}{2},-\frac{1}{2}\right\rangle=\bar{a}''_2, \tag{A25}$$

$$\left|3,-1,\frac{1}{2},-\frac{1}{2}\right\rangle=\frac{\bar{e}'-i\bar{e}'}{\sqrt{2}}, \tag{A26}$$

$$\left|3,-2,\frac{1}{2},-\frac{1}{2}\right\rangle=\frac{\bar{e}''-i\bar{e}''}{\sqrt{2}}, \tag{A27}$$

$$\left|3,-3,\frac{1}{2},-\frac{1}{2}\right\rangle=\frac{\bar{a}'_2-i\bar{a}'_1}{\sqrt{2}}. \tag{A28}$$

Here, $|\psi_{\mathrm{D3h},i}\rangle$ is denoted by the D_{3h} symmetry representation for the corresponding 4f-orbitals, and their spin (α or β) is distinguished by the bar on the orbital (e.g., $a'_2 = a'_2\alpha$ and $\bar{a}'_2 = a'_2\beta$).

Appendix B

SA-CASSCF wavefunctions are expressed as a linear combination of $|\psi_{D3h,i}\rangle$, thus it is easy to derive the Hamiltonian matrix (excluding the spin-orbit coupling terms) with the basis set of **D**; it is expressed as $\mathbf{C}^t\mathbf{E}_0\mathbf{C}$ where $\mathbf{E}_0$ is a diagonal matrix composed of SA-CASSCF energy values and **C** indicates the matrix of CI-coefficients for the respective SA-CASSCF wavefunctions. On the other hand, the spin-orbit-coupling terms are expressed as a diagonal matrix with the basis set of **J** (denoted as $\mathbf{V}_{SO}$) of which components are derived from the atomic SOCs in Table 5 and Eq. (4) and Eq. (6). Then, the total Hamiltonian matrix in terms of the basis set of **D** can be written as

$$\mathbf{H}^{tot} = \mathbf{C}^t\mathbf{E}_0\mathbf{C} + \mathbf{U}_{LD}\mathbf{U}_{JL}\mathbf{V}_{SO}\mathbf{U}_{JL}^t\mathbf{U}_{LD}^t, \qquad \text{(A29)}$$

where $\mathbf{U}_{JL}$ and $\mathbf{U}_{LD}$ denote unitary matrices for the transformations of the basis sets, $\mathbf{J} \rightarrow \mathbf{L}$ and $\mathbf{L} \rightarrow \mathbf{D}$, respectively. Through the diagonalization of $\mathbf{H}^{tot}$, the energies and eigenvectors of the spin-orbit coupled states can be determined in the representation of **D**. The representation of those spin-orbit coupled states can be easily transformed from **D** to **J** using $\mathbf{U}_{JL}$ and $\mathbf{U}_{LD}$ (the transformation matrix for one electron case is given in Appendix A).

References

[1] M. Dolg, H. Stoll, A. Savin, H. Preuss, Theor. Chim. Acta 75 (1989) 173.
[2] R.B. Ross, S. Gayen, W.C. Ermler, J. Chem. Phys. 100 (1994) 8145.
[3] T.R. Cundari, W.J. Stevens, J. Chem. Phys. 98 (1993) 5555.
[4] See, for example, I.N. Levine, Quantum Chemistry Prentice-Hall, NJ, 1991, pp. 309–314.
[5] S. Itoh, R. Saito, T. Kimura, S. Yabushita, J. Phys. Soc. Japan 62 (1993) 2924.
[6] S. Itoh, R. Saito, T. Kimura, S. Yabushita, J. Phys. Soc. Japan 63 (1994) 807.
[7] E. Sanoyama, H. Kobayashi, S. Yabushita, J. Mol. Struct. (Theochem), 451 (1998) 189.
[8] W.DeW. Horrocks, Jr., M. Albin, Prog. Inorg. Chem. 31 (1984) 1.
[9] G. Jeske, H. Lauke, H. Mauermann, H. Schumann, T.J. Marks, J. Am. Chem. Soc. 107 (1985) 8111.
[10] P.L. Watson, G.W. Parshall, Acc. Chem. Res. 18 (1985) 51.
[11] R.B. Lauffer, Chem. Rev. 87 (1987) 901.
[12] C.N.R. Rao, B. Raveou, Acc. Chem. Res. 22 (1989) 106.
[13] R.D. Wesley, C.W. DeKock, J. Chem. Phys. 55 (1971) 3866.
[14] E.W. Kaiser, W.E. Falconer, W. Klemperer, J. Chem. Phys. 56 (1972) 5392.
[15] C.E. Myers, D.T. Graves, J. Chem. Eng. Data 22 (1977) 436.
[16] M. Hargittai, Coord. Chem. Rev. 91 (1988) 35.
[17] K. Hilpert, M. Miller, F. Ramondo, J. Chem. Phys. 102 (1995) 6194.
[18] C.E. Myers, L.J. Norman, II, L.M. Loew, Inorg. Chem. 17 (1978) 1581.
[19] J.C. Culberson, P. Knappe, N. Rösch, M.C. Zerner, Theor. Chim. Acta 71 (1987) 21.
[20] M. Dolg, H. Stoll, H. Preuss, J. Mol. Struct. (Theochem) 235 (1991) 67.
[21] J. Molnár, M. Hargittai, J. Phys. Chem. 99 (1995) 10780.
[22] T.R. Cundari, S.O. Sommerer, L.A. Strohecker, L. Tippett, J. Chem. Phys. 103 (1995) 7058.
[23] S.D. Bella, G. Lanza, I.L. Fragalà, Chem. Phys. Lett. 214 (1993) 598.
[24] G. Lanza, I.L. Fragalà, Chem. Phys. Lett. 255 (1996) 341.
[25] P.J. Hay, W.R. Wadt, J. Chem. Phys. 82 (1985) 299.
[26] M. Dupuis, HONDO 95.1 from CHEM-Station, IBM Corporation, Neighborhood Road, Kingston, NY, 12401, 1995.
[27] W.J. Stevens, H. Basch, M. Krauss, J. Chem. Phys. 81 (1984) 6026.
[28] W.J. Stevens, M. Krauss, H. Basch, P.G. Jaisen, Can. J. Chem. 70 (1992) 612.
[29] M.M. Francl, W.J. Pietro, W.J. Hehre, J.S. Binkley, M.S. Gordon, D.J. DeFrees, J.A. Pople, J. Chem. Phys. 77 (1982) 3654.
[30] H.A. Jahn, E. Teller, Proc. R. Soc. London Ser. A 161 (1937) 220.
[31] E.U. Condon, G.H. Shortley, The Theory of Atomic Spectra, Cambridge University Press, 1951.
[32] M. Gerloch, Orbitals, Terms and States, John Wiley, Chichester, 1986.